Arabian Journal of Chemistry (2021) **14**, 103247

King Saud University

Arabian Journal of Chemistry

www.ksu.edu.sa
www.sciencedirect.com

ORIGINAL ARTICLE

Preparation of superhydrophobic composite paper mulching film

Anling Li [a,b], **Qianrui Kang** [b], **Shuaiyang Ren** [b], **Yong Zhang** [b], **Fengwei Zhang** [a], **Qiang He** [b,*]

[a] *College of Mechanical and Electrical Engineering, Gansu Agricultural University, 730070, China*
[b] *Key Laboratory of Surface Engineering, Anyang Institute of Technology, Anyang 455000, China*

Received 2 May 2021; accepted 1 June 2021
Available online 6 June 2021

KEYWORDS

Superhydrophobic;
Durability;
Mechanical stability;
Chemical stability;
Self cleaning

Abstract To study the influence of different concentrations of zinc oxide (ZnO)/silicon dioxide (SiO_2) composite coating on hydrophobic property and mechanical stability of paper mulch film, three kinds of ZnO/SiO_2 composite coating paper mulch films (2%, 4%, 6%) with different coating substance contents were prepared by brush coating method. Through particle size analysis, contact angle, rolling angle and mechanical stability test, combined with scanning electron microscope, three-dimensional morphology and roughness measuring instrument, the optimal concentration of ZnO/SiO_2 composite coated paper mulch film was screened out. Through acid-base salt corrosion test, silver mirror reaction and surface self-cleaning, the optimal concentration of composite coated paper mulch film was compared with the original paper mulch film to prove its excellent chemical stability and hydrophobicity. The results show that the paper mulch film with 4% coating material has excellent hydrophobicity and mechanical stability, can effectively reduce the surface roughness of paper mulch film, and has remarkable effects in resisting acid, alkali and salt and self-cleaning.

1. Introduction

Paper is a common and indispensable material in daily life, and the characteristics of paper have attracted wide attention. It has low price, renewable, high biodegradability and good mechanical properties. However, paper is very sensitive to water, which often swells or loses its mechanical properties due to water absorption in humid environment. If paper is endowed with good hydrophobicity, it can also have great application in wet environment (Saglam et al., 2017; Martn Closas et al., 2016; Lu et al., 2016; Elsharkawy et al., 2014). In order to protect the existing living environment, many experts and researchers at home and abroad are studying and popularizing the application of paper mulching film in the field (Liu et al., 2010; Li et al., 2020; Pan et al., 2020).

* Corresponding author.
E-mail address: aystar@163.com (Q. He).
Peer review under responsibility of King Saud University.

ELSEVIER Production and hosting by Elsevier

https://doi.org/10.1016/j.arabjc.2021.103247
1878-5352

Because of its excellent surface self-cleaning and antifouling properties, superhydrophobic can be applied to various fields such as architectural coatings, textiles, paper and metal corrosion prevention (Vazirinasab et al., 2018; Verplanck et al., 2007). Therefore, the superhydrophobic property of material surface has become the main research direction in recent years. However, the apparent contact Angle defined by the superhydrophobic surface varies with the surface tension of different liquids (Nguyen et al., 2010). Based on this phenomenon, people began to prepare bionic hydrophobic surfaces according to some biological hydrophobic phenomena in nature, and prepared superhydrophobic surfaces by template method, laser etching method, vapor deposition method and some combination methods (Li et al., 2007). Erbil et al. (2003) prepared superhydrophobic surface by simple gel method based on polypropylene, proper solvent and temperature. Ozbay and Erbil (2015) prepared superhydrophobic SBR surface by spraying grafted SBR solution with silica and spraying it on glass. Gao et al. (2015) prepared super-hydrophobic composite filter paper by micro-adhesion method. The surface of the filter paper was modified by amorphous titanium dioxide nanostructure. The surface energy was low, and the superhydrophobic film structure on the surface of the prepared filter paper was very stable. Spathi et al. (2015) found that superhydrophobic powder with water contact angle greater than 150° can be prepared by stearic acid dry grinding of papermaking sludge ash. Zhang et al. (2015) prepared multiwalled carbon nanotubes (Mwnt) and their silver nanoparticles (AgNP) hybrids by filtration method. After being treated with 1-octadecanol, the silver/Pap hybrid (MPBA) was superhydrophobic. Navarro et al. (2003) prepared fluorinated thin layers on the surface of chemical thermo-mechanical pulp (CTMP) sisal paper with fluorotrimethylsilane (FTMS) as RF plasma. Song et al. (2014) successfully prepared new biodegradable nanocomposites by adding modified nano cellulose fiber (NCF) into biodegradable polylactic acid (PLA) matrix. Jonhed et al. (2010) studied the effect of glycerol addition on the mechanical properties and barrier properties of temperature-responsive hydrophobic modified potato starch on free membrane. Cusola et al. (2013) proposed a new method of hydrophobic cellulose substrate based on existing enzyme technology, which showed that enzyme treatment has the potential to improve the surface hydrophobicity of paper-based media. Cappelletto et al. (2012) studied the sol-gel impregnation coating of siloxane precursor on pure cellulose paper, which showed that the stronger the hydrophobicity of coating sample, the higher the methyl number of siloxane precursor, and it was not affected by the coating thickness. Jyoti et al. (2014) extracted surface wax from the leaves of Boletus and Malus pinnatifida by using various solvents such as ethanol, methanol, benzene and acetone, and made a preliminary study on it. The results showed that the paper tray with benzene as the extract had the highest hydrophobicity (29.57%). Iselau et al. (2015) synthesized three kinds of hydrophobic particles with different charges by emulsion polymerization, namely cationic (SP+), anionic (SP) and amphoteric (SPA), and evaluated their surface hydrophobic properties (commonly called surface sizing). Oh et al. (2011) prepared hydrophobic self-assembled monolayers with silane on paper by a simple and convenient gas-phase or solvent-phase method. The research results show that under different coating methods and silane treatment conditions, the effective reaction time and silane concentration can form stable SAM. Baidya et al. (2017) introduced the preparation of durable and multi-functional super-hydrophobic paper from water-borne fluorinated cellulose nanofiber blocks, and found that the paper made by this method has excellent mechanical durability. In the above-mentioned natural hydrophobic and artificial hydrophobic phenomena, some theoretical models such as Cassie Baxter and Wenzel were used to verify and explain these phenomena in combination with wetting zone transition and roughness influence (Liu et al., 2015; Hisler et al., 2014). Erbil and Cansoy (2009) used Cassie Baxter and Wenzel contact angle theoretical models to compare the theoretical results with the experimental results, and found that Cassie-Baxter theoretical model has better applicability to the contact angle results of superhydrophobic surfaces. However, it is still difficult to control the roughness of hydrophobic surface perfectly and trigger the transition of wettability area (Bhushan and Jung, 2011).

Silicon dioxide (SiO_2) and zinc oxide (ZnO) are hydrophilic particles in the natural state, but after subsequent treatment, both particles can become hydrophobic particles and are widely used in the preparation process of superhydrophobic surfaces (Sun et al., 2019; Ye et al., 2016; Mousavand et al., 2010). Ogihara et al. (2012) prepared superhydrophobic transparent coating on paper by spraying alcohol suspension of nano-SiO_2. Liang et al. (2018) aiming at the poor self-cleaning performance of PTFE film, added hydrophilic SiO_2 particles as filler to PTFE spinning solution, thus changing the surface morphology of PTFE film, and formed multi-stage rough surface through SiO_2 particles, and prepared superhydrophobic PTFE film. Xu et al. (2010) successfully coated the ZnO nanorods with silica particles on the glass surface by hydrothermal method. The introduction of silica particles made the ZnO nanorods have a better uniform and rough structure, which finally made the composite material show excellent hydrophobicity. Ranjbar et al. (2015) attached zinc oxide nanorod arrays on the surface of cotton fabric, and prepared cotton fabric with better superhydrophobic properties after modified by dodecyl trimethoxysilane (DTMS).

To sum up, there are many kinds of preparation technologies related to superhydrophobic, and basically every preparation method has obvious advantages and disadvantages. Rough surfaces prepared by current superhydrophobic preparation methods generally have poor durability (Shirtcliffe et al., 2010). Under the influence of wear, sand and temperature, hydrophobic surface is prone to hydrophobic failure (Erbil, 2020). In view of the practical application of paper mulch film in the field, the hydrophobic surface of paper needs good mechanical durability and chemical stability, but there are few studies on the mechanical durability and chemical stability of paper mulch film.

In this paper, the zinc oxide and silicon dioxide solution were uniformly brushed on the surface of paper mulch film by a very simple brushing process, and a double-layer structure covered by two kinds of coatings was formed on the surface of paper mulch film, thus realizing the surface modification of paper mulch film in different levels. The ZnO/SiO_2 composite coating with the best concentration was selected by measuring contact angle, rolling angle, mechanical stability experiment, scanning electron microscope, three-dimensional topography and roughness measuring instrument. Then, the experiments of acid, alkali and salt corrosion, silver mirror reaction and

self-cleaning were carried out, which proved its excellent hydrophobic performance and chemical stability, and provided theoretical basis for the practical application of hydrophobic paper mulching film.

2. Materials and methods

2.1. Materials

The fully degradable paper base film (Shandong Rebos Tobacco Co, Ltd.) Hydrophobic gaseous SiO_2. Type: HB-139; Main components: hydrophilic SiO_2 and polydimethylsiloxane (PDMS); Particle size: 200 nm; Manufacturer: China Yichang huifu silicon material co., ltd. Nanometer ZnO. Type: DXH-LH30Y; Main ingredients: nano ZnO, stearic acid; Particle size: 300 nm; Manufacturer: China Darcy Nano Technology Co., Ltd. Deionized water, NaOH solution, HCl solution and NaCl solution were all prepared in laboratory.

2.2. Equipment and instruments

HKCA-15 contact angle tester (Beijing Hacker Instrument Factory), electronic balance (AUM220D, Shanghai Tianping Instrument Technology Co., Ltd.), laser particle sizer (Brookhaven, USA), Fourier transform infrared spectroscopy (FTIR, IRTracer-100, Japan), Labram high-resolution Raman spectrometer, X-ray diffractometer, SEM450 field emission scanning electron microscope (FESEM) X-ray diffraction (XRD) instrument (BRUKER, USA).

2.3. Material preparation process

600 ml anhydrous ethanol was measured, 100 ml was added to 6 beakers per serving, 2 g, 4 g, 6 g SiO_2 particles and ZnO particles were weighed by electronic balance, and three different masses of SiO_2 and ZnO were added to the above six beakers containing 100 ml anhydrous ethanol, respectively. Ultrasonic dispersion 15 min to prepare 2%, 4%, 6% ZnO, SiO_2 brush coating solution, three pieces of paper of the same size. The paper mulch film with three different concentrations of ZnO solution as the substrate was prepared by evenly brushing the 2,4,6% ZnO solution with the brush and drying the paper in the drying oven for 15 min. The dried paper mulch film was taken out, and the 2%, 4% and 6% SiO_2 solution was used to brush the surface of the paper mulch film. The paper mulch film after brushing SiO_2 solution was put into the drying oven to dry 15 min. After drying and taking out, three kinds of paper mulch films with different coating concentrations were prepared. Fig. 1 shows the flow chart of 4% paper film sample preparation, and 2% and 6% paper film samples can be prepared by the same method.

2.4. Performance and characterization tests

The contact angle and rolling angle of the base paper, 2%, 4% and 6% paper surface are measured by HKCA- 15 contact angle tester. The drop volume is 4 μl when the surface contact angle is measured, and the droplet volume is 10 μl when the surface rolling angle is measured. The values of contact angle and rolling angle are calculated according to the average values of five points randomly selected on the sample surface. The microstructure of four different concentrations of paper surfaces was observed by SEM450 field emission scanning electron microscope and ST- 400 three-dimensional non-contact surface profiler. The element types and element contents of four different types of paper surfaces were determined by EDS. Laser particle size analyzer (Brookhaven, USA) is used to detect the particle size of SiO_2 and ZnO. The two kinds of particles were qualitatively analyzed by X-ray diffractometer.

3. Results and discussion

3.1. Characterization analysis

3.1.1. XRD analysis

The red dots in Fig. 2(a) are the diffraction peaks of ZnO. By observing Fig. 2(a), it can be found that there are a total of 11 diffraction peaks of ZnO, and the rest diffraction peaks are related products of nano-sized zinc oxide after stearic acid treatment. According to the half-height width of the diffraction peak, the narrower the half-height width, the higher the crystallinity and the larger the grain size. As can be seen from Fig. 2 (a), the half-height and width of the 11 diffraction peaks belonging to ZnO are different, which indicates that the processed ZnO is not formed in regular shape (Khaghanpour and Naghibi, 2017). Fig. 2(b) is the diffraction peak map of SiO_2. An obvious characteristic peak was found at $2\theta = 24°$, which shifted relative to the 22° in the standard JCPDS card, mainly because the silica used was modified by PDMS. At the same time, it is confirmed that the SiO_2 in SEM has obvious lamellar structure.

3.1.2. Particle size analysis

Fig. 3 (a) shows the distribution of ZnO particle groups with different particle sizes in the powder. It can be seen that the particle size of ZnO particle group is concentrated in the range of 200 nm ~ 500 nm, in which the particle size of 263–314 nm is the most. Fig. 3 (b) shows the distribution of SiO_2 particle group with different particle size in the powder. From Fig. 3 (b), we can see that most of the particle size of SiO_2 particle group is concentrated in the range of 207–236 nm, and there are more particles in the range of 162–187 nm. Through this experiment, the uniformity of ZnO and SiO_2 particle size can be reflected, and the numerical set of the proportion of particles of different sizes in the whole can be calculated from the particle size distribution diagram of Fig. 3.

3.1.3. Particle morphology analysis

Fig. 4(a) and (c) are low power scanning electron microscope images of ZnO and SiO_2, respectively. Through the local magnification of Fig. 4(b) and (d), we can find that there are obvious differences in microscopic morphology between zinc oxide and silicon dioxide. Zinc oxide is irregular short rod-shaped, while silicon dioxide is irregular flake structure, relative to the paper mulch film coated with silica alone. Particles on the surface of paper mulch film coated with zinc oxide and then silicon dioxide are more closely combined with the paper surface. It is not easy for each particle to agglomerate, and a relatively large air gap will be formed between particles. In this way, Cassie-Baxter model can be established on the

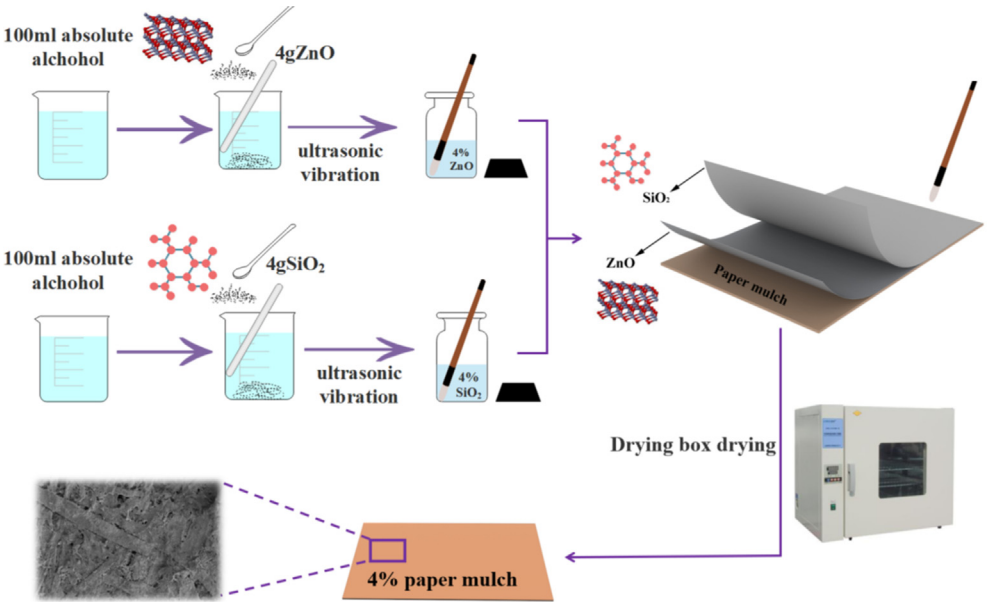

Fig. 1 Preparation process of superhydrophobic surface of paper mulching film with coating concentration of 4%.

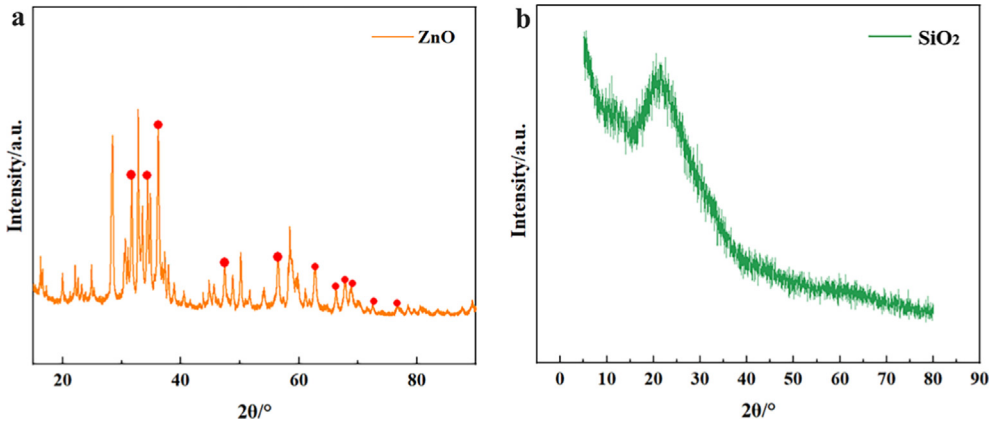

Fig. 2 (a) XRD of ZnO; (b) XRD of SiO_2.

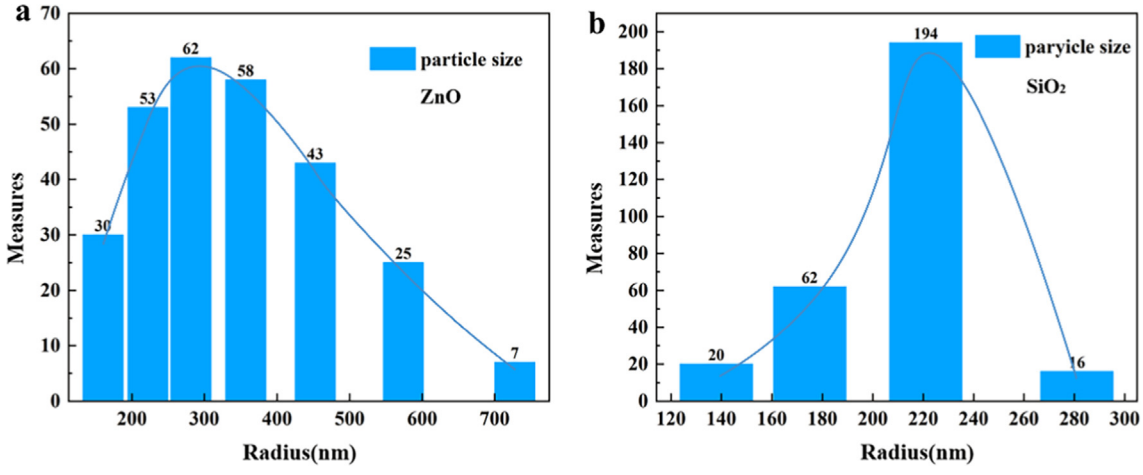

Fig. 3 (a) The particle size of ZnO and (b) the particle size of SiO_2.

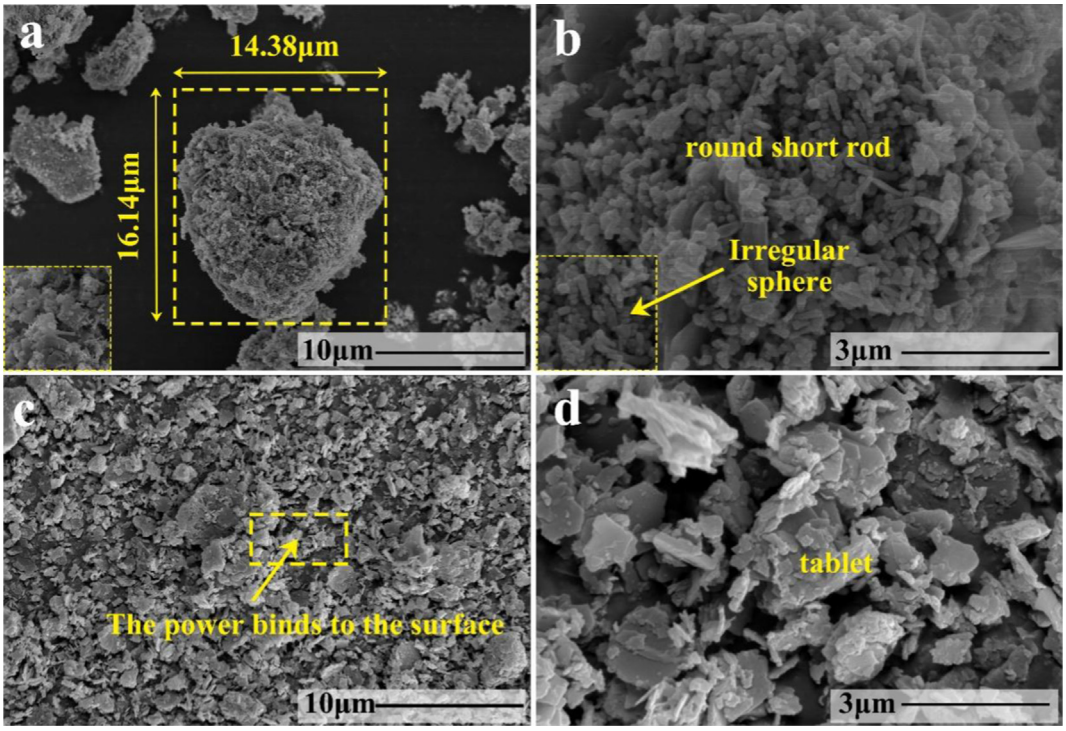

Fig. 4 (a) Low magnification electron microscope picture of ZnO; (b) High power electron microscope picture of ZnO; (c) Low magnification electron microscope picture of SiO_2; (d) High power electron microscope picture of SiO_2.

microstructure of zinc oxide and silicon dioxide particles exposed outside the paper mulch film. Make the surface of the coating superhydrophobic.

3.2. Hydrophobicity and durability of paper mulching film surface

3.2.1. Performance test of contact angle and rolling angle

Fig. 5 shows three different states of droplets on different paper surfaces. The change of the contact angle between droplets and the paper surface is mainly due to the different tension at the solid-liquid-vapor interface. Fig. 5 (d) shows the Wenzel state of droplets on the paper surface. Because the tiny holes on the paper surface enhance the wettability of the paper surface, the droplets wet the paper surface, and the tiny gaps on the paper surface are completely filled with droplets. Fig. 5 (c) depicts a transition state in which the droplet is between the Wenzel state and the Cassie state, and there is an adhesion between the paper and the droplet, which increases with the depth of the droplet infiltrating into the paper surface. Fig. 5 (b) shows the Cassie state. Between the liquid and the rough paper surface, the droplets are not fully filled on the rough paper surface. This contact is a compound contact composed of solid-liquid contact and gas-liquid contact. It is found that in this contact state, reducing the solid-liquid contact area can improve the hydrophobic effect of the paper surface. On the basis of Wenzel theory and Cassie theory, increasing the rough structure of the paper surface or reducing the solid-liquid contact area can make the paper surface more hydrophobic.

In order to study the effect of brushing ZnO/SiO_2 composite coating on paper mulch film on its contact angle and rolling angle, the contact angle and rolling angle were measured on the surface of original paper mulch film and three kinds of paper mulch film with different concentration of coating material. As shown in Fig. 6 (a), the contact angle of the original paper mulch film is 131°, which shows that the original paper has a certain hydrophobicity, but it can be seen from the rolling angle that when the rotation angle is 90°, the droplets of 10 μl still cannot roll off on the paper surface, indicating that the original paper mulch film has great adhesion to water droplets. Two tests show that the original paper mulch film is not superhydrophobic. Fig. 6 (b) shows that the contact angles of the paper mulch films with 2%, 4% and 6% coating material content are all greater than 150°, and show a trend of rising at first and then decreasing, in which the contact angle with 4% coating material content is the largest, reaching about 161°. Fig. 6

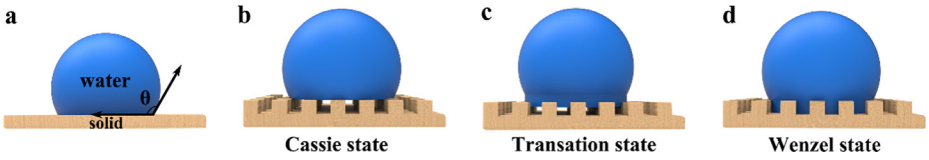

Fig. 5 Wetting state of water droplets on different surfaces; (a) Young's state; (b) Cassie state; (c) Transition state; (d) Wenzel state.

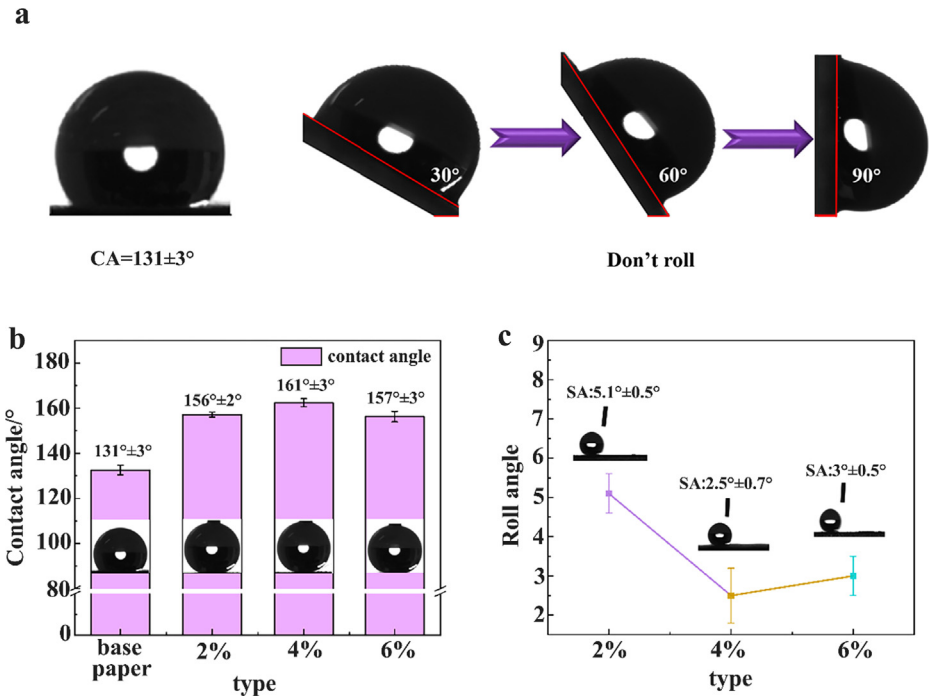

Fig. 6 (a) Contact angle and rolling angle (90°) of base paper cannot roll off (b) contact angle of four kinds of paper; (c) schematic diagram of rolling angle of 2%, 4% and 6%.

(c) reflects the rolling angle of 2%, 4% and 6% of the sample, and the roll angle decreases at first and then increases, and the roll angle of 4% is the smallest. At about 2.5°, the contact angles of the three kinds of paper are all less than 10°. Combined with Fig. 6 (b), it can be seen that the paper mulch films with different coating contents can meet the requirements of superhydrophobicity. The reason for this excellent hydrophobicity is mainly due to the formation of Cassie model after the droplets on the surface of the paper mulch film come into contact with the rough structure of the sample surface. The combination of Fig. 6 (b) and Fig. 6 (c) shows that the contact angle with 4% coating material content is the largest, while the rolling angle is the smallest compared with the other two. To sum up, the hydrophobic performance of the coating with 4% coating material content is better.

3.2.2. Test and analysis of stability friction

Fig. 7 (a) is a schematic diagram of the paper mulch film durability friction test and the change of the contact angle curve after friction. The contact angle data were measured every 10 cm. The contact angle of the paper mulch film with 2% coating content decreased to 147° after three friction cycles (running 30 cm), the coating no longer had superhydrophobicity, and the contact angle of the paper mulch film with 4% coating content decreased to 148° after 7 friction cycles (running 70 cm). The coating is no longer superhydrophobic. After 4 times of friction cycles, the contact angle of the paper mulch film with 6% coating material content is reduced to 148°, and the contact angle of the first eight groups of 4% coating material is larger than that of the coating with 2% and 4% coating material content. According to Fig. 7 (c), the average percentage of contact angle of paper mulch film with 2% coating material decreased by 1.94%, that of paper mulch film with 4% coating material decreased by 1.93%, and that of paper mulch film with 6% coating material decreased by 2%. And the paper mulch film with 4% coating material content does not have superhydrophobic after 7 friction cycles, and the number of friction cycles is the highest compared with the other two kinds of paper mulch film, It shows that the paper mulch film with 4% coating material content has better hydrophobicity and stability.

3.2.3. Experimental analysis of stability adhesive tape

Mechanical stability is an important index to evaluate the comprehensive performance of paper mulch film. Fig. 8 shows the experimental process of paper mulch tape uncovering experiment. First, the paper mulch film with different concentrations of coating is fixed on the glass slide by double-sided glue, and then the paper mulch tape is glued to the surface of the paper mulch film. The weight of 0.5 kg is placed on the surface of the paper mulch film for about 1 min, the weight is removed, and the tape covering the surface of the paper mulch film is torn slowly. After tearing, obvious burrs can be observed on the surface of the paper mulch film, indicating that the surface structure of the paper mulch film has been destroyed.

It can be seen from Fig. 9 that the contact angle of the paper mulch film with 2% coating material content decreased from 156° to 145° after two adhesive tapes, and the coating no longer has superhydrophobic properties. After three times of taping, the contact angle of the paper mulch film with 4% coating material content decreased from 161° to 149°, and the coating no longer had superhydrophobic property. After four times of taping, the contact angle of the paper mulch film with 6% coating material content decreased from 158° to 147°, and the coating no longer had superhydrophobic property.

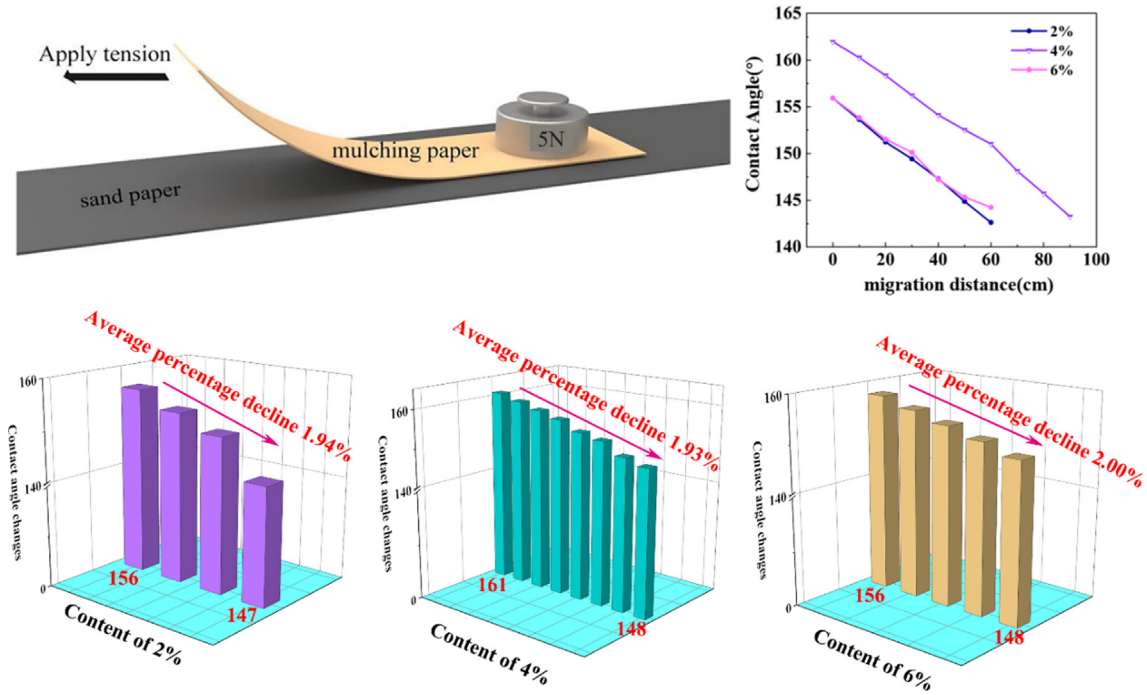

Fig. 7 (a) Schematic diagram of friction test for stability of paper mulch film; (b) Changes of wear times and contact angle of three kinds of paper; (c) Bar chart of average decline percentage of contact angle of three kinds of paper.

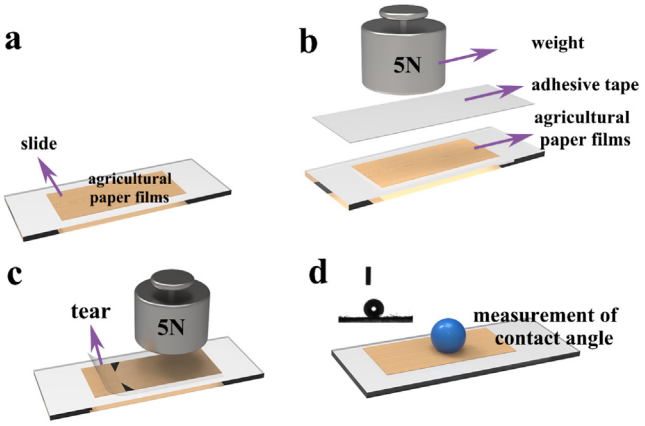

Fig. 8 Schematic diagram of adhesive test of paper mulching tape. (a), (b), (c) and (d) are the sequence of the experiment.

The number of adhesive exposures according to the coating material content from high to low is 2% (2 times), 4% (3 times) and 6% (2 times). It can be seen that the paper mulch film with a coating material content of 4% has the most adhesive exposure times, which is four times. This also shows that the paper mulch film with a coating material content of 4% has a good performance of anti-adhesive tape, and its stability is better than that of the other two concentrations of paper mulch film.

3.2.4. Taber wear performance test

As shown in Fig. 10 (a), the Taber wear tester is used to test the mechanical stability of three kinds of paper mulch films with different coating material content. Fig. 10 (b) is the experimental schematic diagram. First of all, the paper mulch film is cut into a circular sample, and the paper mulch is fixed on the base of the testing machine with a metal ring. There are two rollers

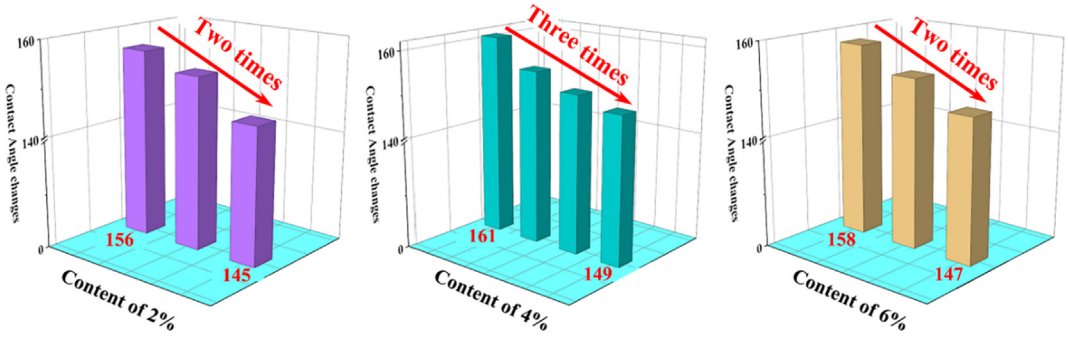

Fig. 9 Histogram of average decreasing percentage of contact angle of three kinds of paper.

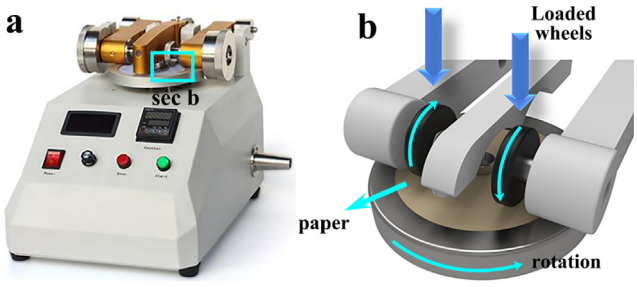

Fig. 10 (a) Taber wear tester; (b) Partial enlarged view of Taber wear tester.

on the testing machine. The roller is put down and pressed on the circular sample of the paper mulch, and the rotation switch is started. A force of 2.5 N is applied on both sides of the roller. With the rotation of the bottom disc, the two rollers have a friction effect on the paper mulch, which changes to a range of 50 revolutions. Measuring the change of contact angle of paper mulch film with different content of three kinds of coating material after friction.

It can be seen from Fig. 11(a) that the contact angle of paper mulch film with 2% coating material decreased to 145° after 50 Taber abrasion cycles, while the contact angle of paper mulch film with 4% coating material after 50 Taber abrasion cycles was 156°, still above 150°. Observation fig. (b) shows that the contact angle of paper mulch film with 6% coating material is still greater than 150° after 50 Taber wear cycles, while the contact angles of 4% coating material and 6% coating material decrease to 147° and 144° respectively after 100 Taber wear cycles, and the contact angle of paper mulch film with 4% coating material content is still larger. To sum up, the paper mulch film with coating material content of 4% has the strongest wear resistance.

3.3. Electron microscopy and EDS analysis of paper mulching film surface

3.3.1. Macro morphology analysis of paper mulching film

As shown in Fig. 12 (a), dense fiber distribution was observed on the surface of the paper mulch film with a coating content of 2%, indicating that the SiO_2 coating did not completely cover the surface of the paper mulch film. By observing the electron microscope picture of the paper mulch film with 4% (b), coating material in Fig. 12, the surface of the paper mulch film is relatively flat, the coating material is evenly distributed on the surface, no obvious fiber distribution is observed on the coating surface, and the macroscopic morphology of the paper mulch film with 4% (e) (coating material is not significantly different from that of the paper mulch film in Fig. 12 (d) (2%). It is inferred that the hydrophobicity of the paper mulch film with the coating material content of 4% is better than that of the paper film with the coating material content of 2%. As shown in Fig. 12 (c) and (f), the electron microscope and macroscopic topography of the paper mulch film with 6% coating material content have observed a large number of obvious cracks on the coating surface and obvious shedding traces of the coating, indicating that the paper mulch film with 6% coating material content has poor stability and poor hydrophobicity at the place where the coating falls off. Too much coating material content may affect the adhesion between the coating and the paper surface, thus affecting the hydrophobic performance of the paper mulch film. Observe the distribution map of elements on the surface of paper mulch film (take Si as an example). As shown in Fig. 12 (g), the distribution of Si element on the surface of 2% paper mulch film is relatively uniform, and the uniformly distributed Si element can be clearly seen on the energy spectrum. Fig. 12 (h) shows the element distribution on the surface of paper mulch film with 4% coating material. The distribution of Si elements on the surface of 4% paper mulch film is significantly more than that of paper mulch film with 2% coating material content, and the distribution of Si on the surface is more uniform. According to Fig. 12 (i) and (l), it can be seen that the distribution of elements on the surface of paper mulch film with 6% coating material content is extremely uneven, which may be related to the shedding of coating surface material. Based on the above results, it is speculated that the hydrophobicity of paper mulch coating with 4% coating material may be better.

3.3.2. Micro-electron microscopic analysis of the surface of paper mulching film

As shown in Fig. 13 (a), dense fiber distribution was observed on the surface of the paper mulch film with 2% coating mate-

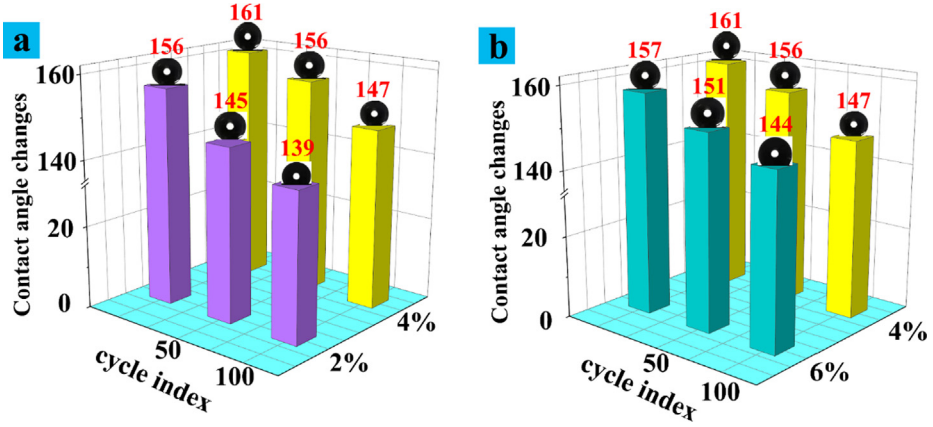

Fig. 11 (a) Histogram of contact angle change after friction between 4% coating and 2% coating; (b) Histogram of contact angle change after friction between 4% coating and 6% coating.

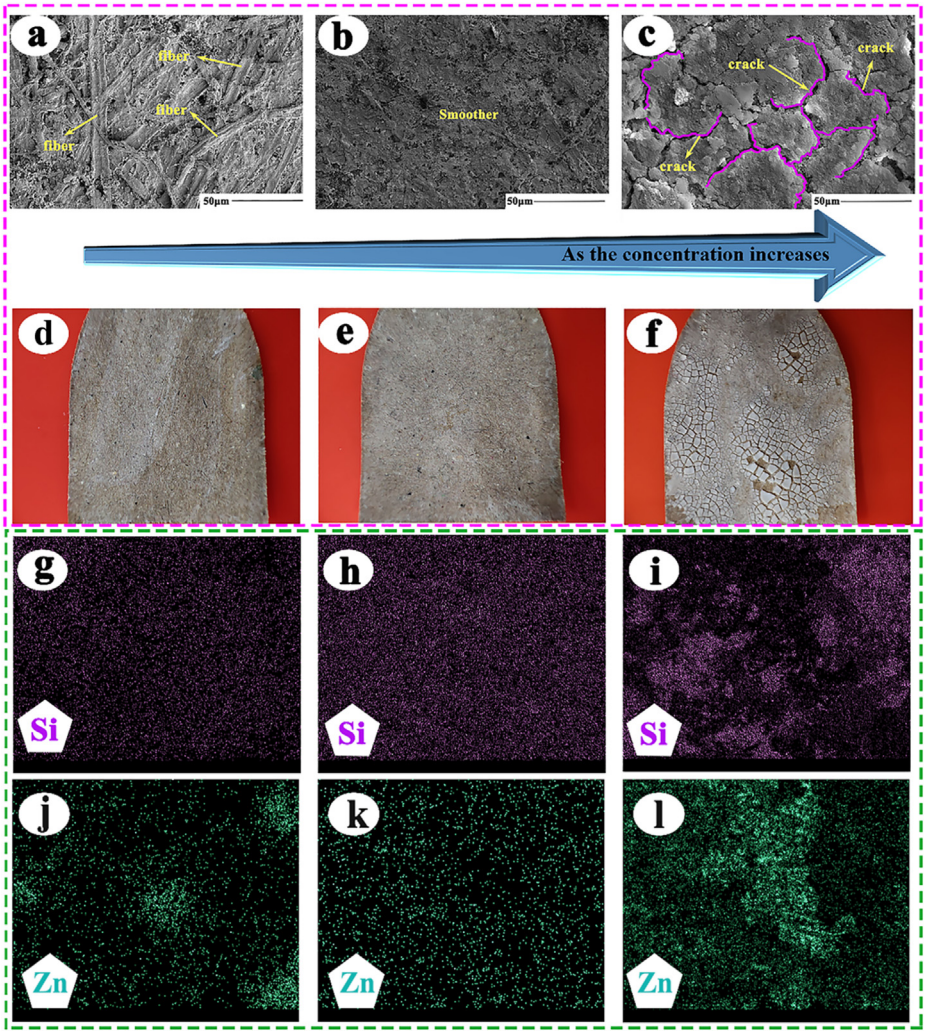

Fig. 12 (a), (b) and (c) are scanning electron microscopic morphologies with coating material content of 2%, 4% and 6%, respectively. The macroscopic topography of paper mulch film with (d), (e) and (f) corresponding to 2%, 4% and 6% scanning electron microscope respectively. (g), (h) and (i) are the energy spectra of the distribution of Si elements at 2%, 4% and 6% on the surface of paper mulch film. (j), (k) and (l) are the energy spectra of the distribution of Zn elements at 2%, 4% and 6% on the surface of paper mulch film.

rial, indicating that the SiO_2 and ZnO coatings did not completely cover the surface of the paper mulch film. Fig. 13 (c) is a magnified view of the fiber on the surface of Fig. 13 (b). It can be observed that although there are particles on the surface, the particle distribution is small and the particle distribution is extremely uneven. According to this phenomenon, it is inferred that although the surface hydrophobicity of different areas of paper mulch film with coating material content of 2% is different, even there are great differences. As shown in Fig. 13 (d), (e), (f), the electron microscope picture of the paper mulch film with 4% coating material content is observed. The surface of the paper mulch film is relatively flat, the coating material is evenly distributed on the surface, and no obvious fiber distribution is observed on the coating surface. The distribution of (f) in Fig. 13 is relatively uniform relative to the 4% paper mulch film particles in the paper mulch film with 2% coating material. According to the electron microscope and macroscopic morphology of the paper mulch film with 6% coating material content of Fig. 12 (f) and (g), a large number of obvious cracks on the coating surface and obvious peeling marks of the coating were observed. According to the observation of Fig. 13 (h) and (i), a large number of particles were found to agglomerate, indicating that the paper mulch film with 6% coating content had poor stability and poor hydrophobicity at the place where the coating fell off. Too much coating material content may affect the adhesion between the coating and the paper surface, thus affecting the hydrophobic performance of the paper mulch film.

3.3.3. Micro-element analysis on the surface of paper mulching film

Because the core elements in the layer covered by paper mulch film are Si and Zn, the coatings on the surface of three kinds of paper mulch film are analyzed by the element distribution of Si and Zn. By comparing Fig. 14 (b), (e) and (h), it is found that the distribution of Si element is less on the surface of paper mulch film with 2% coating material, and the distribution of Zn element in some positions of paper mulch film surface can-

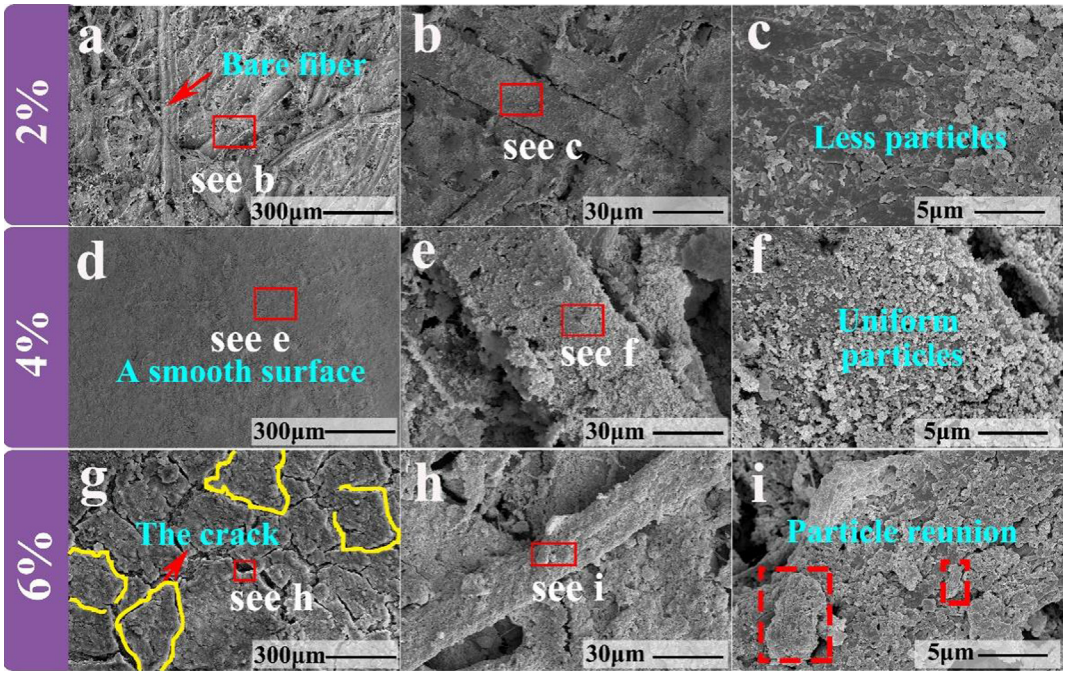

Fig. 13 (a), (b) and (c) are the step-by-step magnification of the scanning electron microscope micro-morphology of the paper mulch film with 2% coating material content, (d), (e) and (f) are the step-by-step magnification of the scanning electron microscope micro-morphology of the paper mulch film with 4% coating content. (g), (h) and (i) are the step-by-step magnification of the scanning electron microscope micro-morphology of the paper mulch film with 6% coating material content.

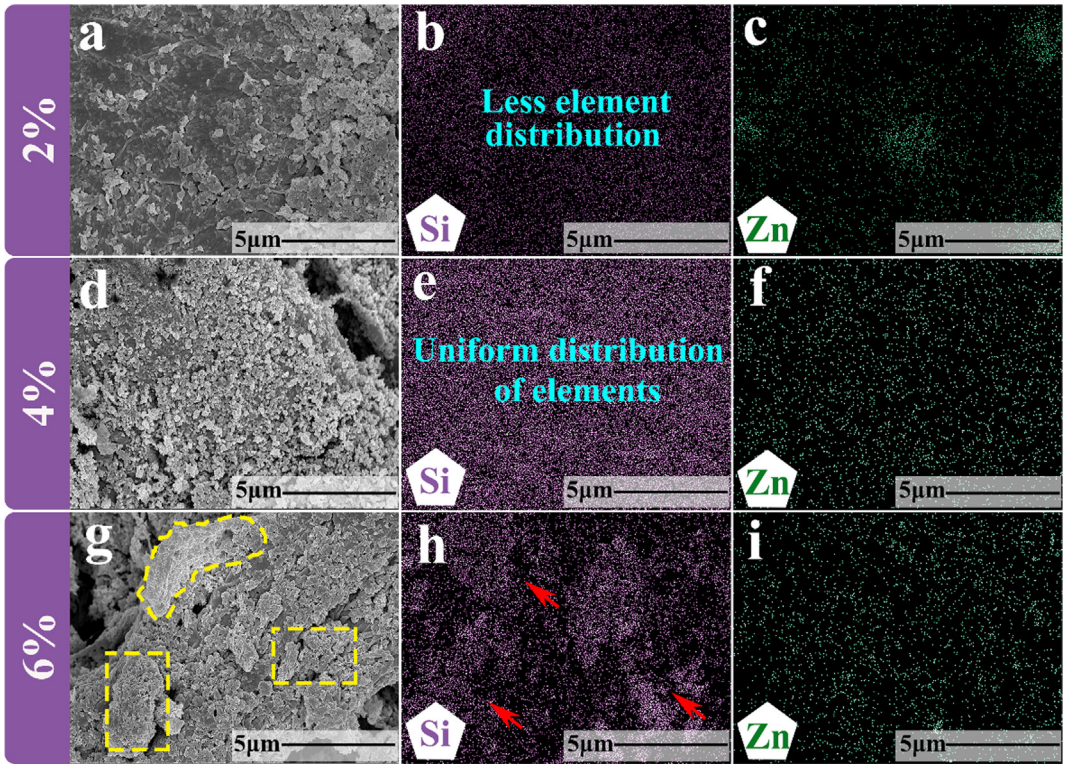

Fig. 14 (a) Surface energy spectrum scanning area of paper mulch film with coating material content of 2%;(b) and (c) distribution of Si and Zn elements on paper mulch film surface with coating material content of 2%,;(d) surface energy spectrum scanning area of paper mulch film with coating material content of 4%,;(e) and (f) surface of paper mulch film with coating material content of 4%;(g) Surface energy spectrum scanning area of paper mulch film with coating material content of 6%;(h) and (i) are the distribution of Si and Zn elements on the surface of paper mulch film with 6% coating material.

not even be observed in Fig. 14 (c). This further illustrates the instability of the hydrophobicity of the paper mulch film with a coating material content of 2%. Compared with the paper mulch film with the coating material content of 2% and 6%, the Si and Zn elements of the 4% paper mulch film are evenly distributed on its surface, and there is no obvious element aggregation and element dispersion. According to the observation of Fig. 14 (g), it was found that there was a large number of particle agglomeration on the fiber surface of paper mulch film with 6% coating material content, and the particle agglomeration phenomenon of Fig. 14 (g) corresponds to the Si element distribution map of Fig. 14 (h), which shows that 6% Si and Zn elements of paper mulch film accumulate on the surface of paper mulch film fiber with this concentration.

3.4. Three-dimensional roughness analysis

The surface roughness of three different concentrations of coatings was measured by interferometric three-dimensional profiler and roughness measuring instrument. In contrast, after the introduction of SiO_2 and ZnO coatings, a large number of zinc oxide and silica particles were attached to the fibers and fiber surfaces of the paper mulch film. These particles on the paper film surface prevent the droplets from directly contacting with the fibers on the paper film surface, and form a Cassie model after the droplets on the paper film surface come into contact with the rough structure of the sample surface, thus improving the contact angle between the paper film surface and the water droplets, and then improving the hydrophobicity of the paper film surface. The arithmetic average height Sa of the surface of paper mulch film with 2% coating material content is 4.480 μm measured by surface roughness measuring instrument. by observing Fig. 15 (b) (three-dimensional topography enlarged view), it is found that there are certain convex structures on the surface of paper mulch film with 2% coating material content, but the height distribution of these convex structures is uneven, because the surface is covered with less SiO_2 and ZnO particles, and the particles do not completely cover the surface of paper mulch film. By observing Fig. 15 (f), it can be found that the arithmetic average Sa of the surface of 4% paper mulching film with coating material content measured by the surface roughness measuring instrument is

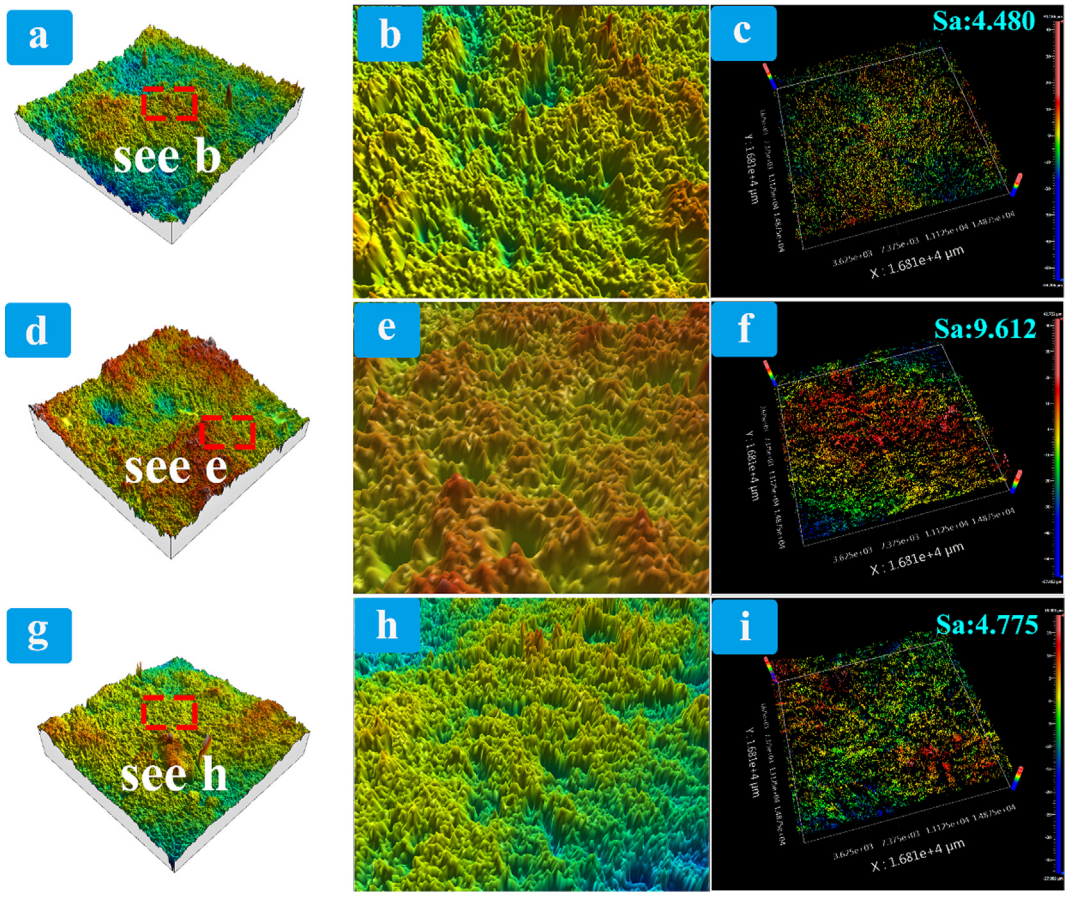

Fig. 15 (a) Three-dimensional morphology of paper mulch film surface with 2% coating material content, (b) enlarged picture of scanning area of paper mulch film surface with 2% coating material content, and (c) measurement picture of surface roughness of paper mulch film with 2% coating material content. (d) Three-dimensional morphology of paper mulch film surface with coating material content of 4%, (e) enlarged picture of scanning area of paper mulch film surface of 4%, and (f) surface roughness measurement picture of paper mulch film of 4%. (g) three-dimensional morphology of paper mulch film surface with 6% coating material content, (h) enlarged picture of scanning area of paper mulch film surface with 6% coating material content, and (i) 6% measurement map of surface roughness of paper mulch film.

9.612 μm, which is 5.132 μm higher than that of 2% paper mulching film. This is because the disorderly distribution of fibers on the surface of paper mulching film and the existence of interfiber voids, so that silica particles and zinc oxide particles will be scattered between fibers and on the surface of fibers. Due to the addition of more SiO_2 and ZnO particles, the fiber cracks on the surface of paper mulching film are filled by more particles, and these rough particles are evenly covered on the surface of paper mulching film. Therefore, the surface roughness of paper mulching film with the addition amount of 4% will be improved compared with that with the addition amount of 2%. According to Fig. 15 (e), compared with the 2% paper mulching film surface, it can be observed that the surface has a relatively uniform and sharp convex structure, indicating that SiO_2 and ZnO particles form a good rough structure on the 4% paper mulching film surface, and the excellent hydrophobic performance of the coating surface is also verified through experiments. According to the surface roughness measurement instrument, the arithmetic average Sa of the surface of the paper mulching film with the coating content of 6% is 4.775 μm. Compared with the surface roughness of the paper mulching film with the coating content of 4%, the roughness of the paper mulching film also decreases. By observing Fig. 15 (g), it was found that the particles on the surface of the paper mulching film were not filled evenly. This was because the excessively high concentration of brushing caused cracks on the surface, resulting in a large number of particles falling off, leading to the uneven particle roughness structure on the surface of paper mulching film. The roughness of SiO_2 and ZnO particles is the highest when the dosage of SiO_2 and ZnO is 4%, which is consistent with the results of Cassie model based on the above contact Angle test, hydrophobic stability test and roughness comparison, that is, the surface of paper mulching film is rougher when the dosage of SiO_2 and ZnO particles is 4%. Therefore, it is easier to form hydrophobic structure on the surface of paper mulching film with 4% addition.

3.5. Acid, alkali and salt contact angle corrosion test

Because the application of paper mulch film is in the natural environment, the soil and crops in the natural environment are often corroded by acid rain, resulting in reduced production, so this experiment simulated the corrosion resistance of paper mulch film under the condition of acid, alkali and salt. The experimental steps are as follows: acid, alkali and salt droplets are dropped on the surface of paper mulch with 4% coating material. Fig. 16 (b) shows the morphology of acid, alkali, salt and distilled water on the surface of base paper and paper mulch film with 4% coating material. Fig. 16 (c) and (b) show the change of contact angle of base paper and 4% paper mulch film after soaking in acid, alkali and salt droplets for 24 h and 48 h, respectively. After soaking in acid, alkali and salt for 48 h, the contact angle of the base paper decreased from 133° to 118°, 113° and 128° respectively. After soaking in acid, alkali and salt, the contact angle of the paper mulch film with 4% coating material decreased from 161° to 144°, 143° and 154°, respectively. The contact angle decreased obviously at 24 h and 48 h, which indicated that the alkali resistance of paper mulch was poor. However, the contact angle of the paper mulch film with 4% coating content is still more than 150° after soaking in NaCl for 24 h and 48 h and under acidic

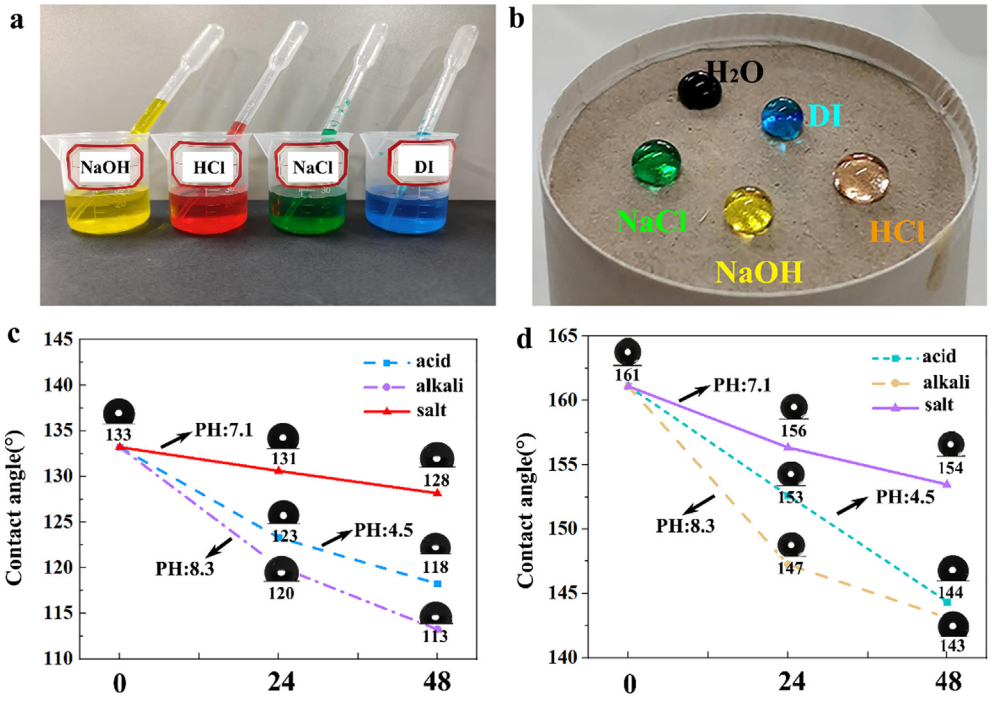

Fig. 16 (a) Acid-base salt solution; (b) the state of acid-base salt on paper mulching film with 4% substance content; (c) the change of contact angle of base paper after soaking in acid-base salt solution; (d) the change of contact angle of paper mulching film with 4% coating substance after soaking in acid-base salt solution.

condition for 24 h, indicating that the paper mulch film with 4% coating content has excellent chemical corrosion resistance.

3.6. Silver mirror reaction experiment

This experiment is a silver mirror reaction experiment, the purpose of which is to observe the phenomenon of paper mulch in distilled water. As shown in Fig. 17 (a), when the paper does not invade the distilled water, the surface of the paper shows the original color of the paper. As shown in Fig. 17 (b) and (c), when the paper is just immersed in distilled water and completely immersed in distilled water, there is an obvious silver mirror phenomenon on the paper surface, and the silver mirror phenomenon is uniformly distributed on the paper film surface, and this phenomenon can be observed everywhere on the paper film surface, indicating that the coating is uniformly distributed on its surface and has excellent hydrophobicity.

3.7. Self-cleaning performance test

Fig. 18 is an experimental step diagram of the self-cleaning device. The paper mulching film with a layer of soil on the surface is adhered to the glass slide, and the distilled water is dripped on the surface of the soil with a dropper. After the distilled water rolls off, the surface of the paper mulching film is observed.

Fig. 19 shows the experimental process of superhydrophobic self-cleaning of two kinds of paper mulch films: when the particles are small, the interface force of the superhydrophobic surface is much greater than the adhesion force, and when the deionized water is in contact with the particles, the particles quickly enter the liquid surface under the action of the liquid surface energy. The particles do not stay on the solid surface. Fig. 19 (a-f) shows the test process of self-cleaning of paper mulch with 4% material content of base paper and coating material. Fig. 19 (c), when deionized water drips on the surface of the original paper mulch film, the liquid droplets infiltrate the surface of the paper mulch film, and the water droplets adhere to a part of the fine soil when they come into contact with the fine soil, and cannot slip off under the hindrance of the soil. As shown in Fig. 19 (f), when deionized water drops on the surface of the sample with a coating material content of 4%, the droplets roll off naturally, and it can be seen that the water droplets soak the fine soil in the rolling process. The observation of Fig. 19 (f) shows that the fine soil is taken away from the sample surface, and no traces of paper contamination are found on the paper surface. ZnO/SiO_2 coating endows the surface of paper mulch with superhydrophobic property. When the fine soil particles are small enough, the interfacial force on the surface of ZnO/SiO_2 paper mulch film is greater than the adhesion force, and the spread of liquid droplets under the action of gravity makes the fine soil particles adhere to the surface of deionized water and slip rapidly, indi-

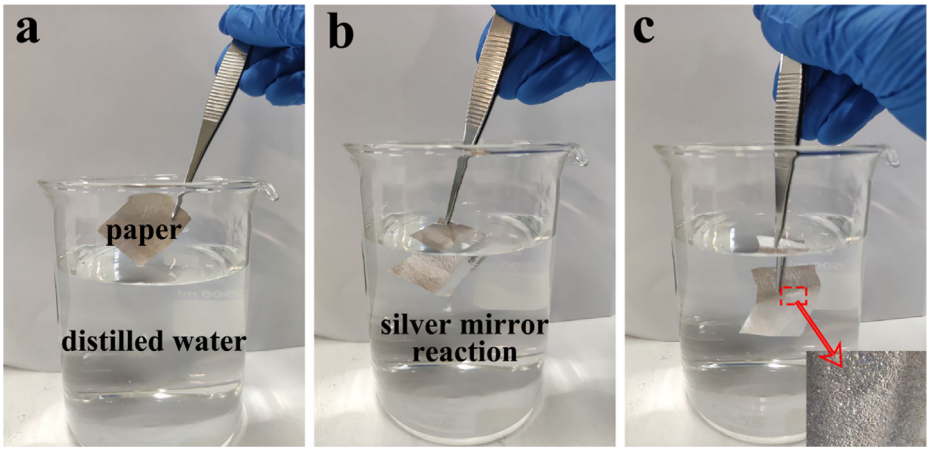

Fig. 17 (a) Paper mulching film without distilled water,;(b) paper mulching film just immersed in distilled water; (c) paper mulching film in distilled water (partial enlarged view).

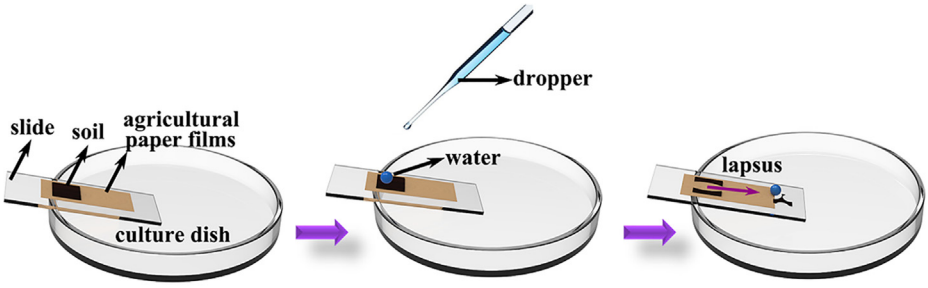

Fig. 18 Experimental step diagram of self-cleaning experimental device.

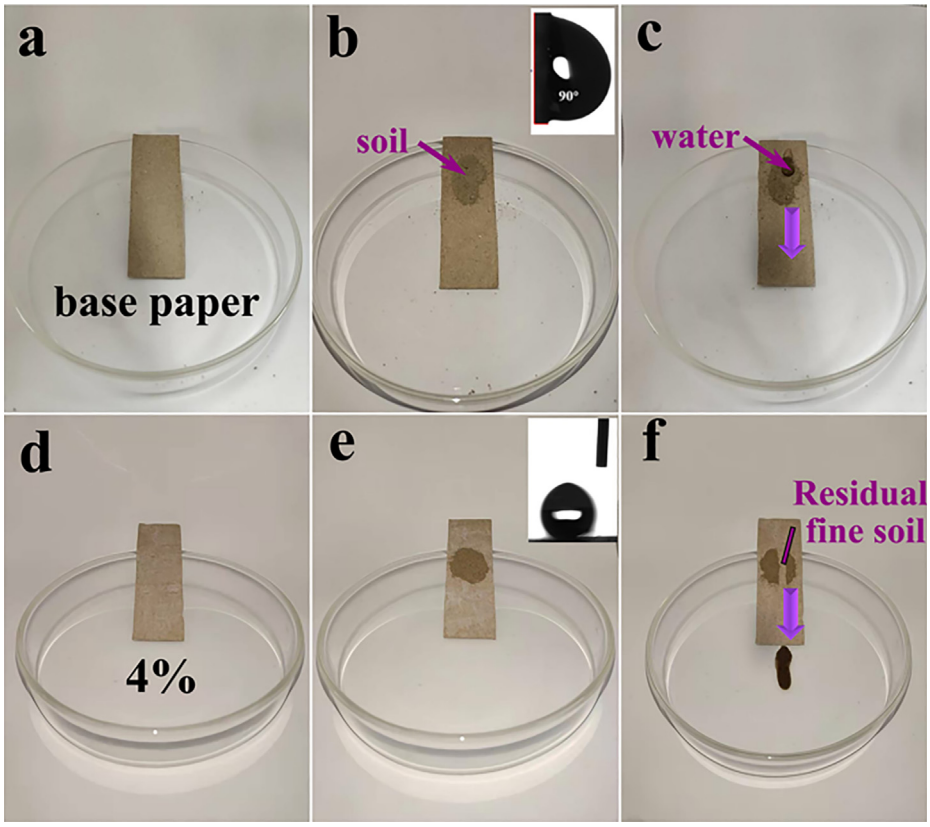

Fig. 19 Phenomenon diagram of self-cleaning experiment.

cating that the surface of ZnO/SiO_2 paper mulch film has good hydrophobicity and less adhesion, so the surface remains dry all the time. To achieve the effect of self-cleaning.

4. Conclusion

The ZnO/SiO_2 composite coating was prepared by simple brushing process with zinc oxide and silicon dioxide as raw materials. The coating has superhydrophobicity on the surface of paper mulch film. Due to the different concentration of brushing solution, the hydrophobic properties of the three kinds of paper mulch films are different. Among them, the paper mulch film with coating material content of 4% has larger static contact angle, smaller rolling angle and better superhydrophobic performance. Scanning electron microscope and EDS were used to observe the surface of paper mulch film. It was found that the surface of 4% composite coating was flatter and the distribution of elements was more uniform. Experiments show that the mechanical durability of 4% composite coating is better, and the self-cleaning performance of the surface of zinc oxide/silicon dioxide composite paper mulch film material with 4% coating substance content is better, and the adhesion to droplets is smaller.

Funding

This research project was supported by the scientific and technological innovation talents of universities in Henan Province (19HASTIT023). The raw/processed data required to reproduce these findings cannot be shared at this time due to legal or ethical reasons.

Declaration of Competing Interest

The authors declare that they have no known competing financial interests or personal relationships that could have appeared to influence the work reported in this paper.

References

Saglam, M., Sintim, H.Y., Bary, A.I., et al, 2017. Modeling the effect of biodegradable paper and plastic mulch on soil moisture dynamics. Agric. Water Manag. 193, 240–250.

Martn Closas, L., Costa, J., Cirujeda, A., et al, 2016. Above-soil and in-soil degradation of oxo- and bio-degradable mulches: A qualitative approach. Soil Res. 54 (2), 225.

Lu, C.P., Tian, Y.L., Ma, Q.B., 2016. Research advance and development prospect of paper Mulch. J. Hui Agric. Sci. 44 (5), 95–96.

Elsharkawy, M., Schutzius, T.M., Megaridis, C.M., 2014. Inkjet patterned superhydrophobic paper for open-air surface microfluidic devices. Lab Chip 14 (6), 1168–1175.

Liu, M., Huang, Z.B., Yang, Y.J., 2010. Analysis of biodegradability of three biodegradable Mulching films. J. Polym. Environ. 18 (2), 148–154.

Li, H., Jiang, Y.H., Han, W.J., et al, 2020. Preparation and properties of degradable plant fiber agricultural film paper. Jiangsu Agric. Sci. 48 (6), 189–194.

Pan, Y., Zheng, M.C., Zhou, Z.X., et al, 2020. Research status and development of biodegradable agricultural film. Guangzhou Chem. Ind. 48 (9), 37–39.
Vazirinasab, E., Jafari, R., Momen, G., 2018. Application of superhydrophobic coatings as a corrosion barrier: A review. Surf. Coat. Technol. 341, 40–56.
Verplanck, N., Coffinier, Y., Thomy, V., et al, 2007. Wettability switching techniques on superhydrophobic surfaces. Nanoscale Res. Lett. 2 (12), 577–596.
Nguyen, T.P.N., Brunet, P., Coffinier, Y., et al, 2010. Quantitative testing of robustness on super-omniphobic surfaces by drop impact. Langmuir 26 (23), 18369–18373.
Li, X.M., Reinhoudt, D., Crego-Calama, M., 2007. What do we need for a superhydrophobic surface? A review on the recent progress in the preparation of superhydrophobic surfaces. Chem. Soc. Rev. 36, 1350–1368.
Erbil, H.Y., Demirel, A.L., Avci, Y., et al, 2003. Transformation of a simple plastic into a superhydrophobic surface. Science 299, 1377–1380.
Ozbay, S., Erbil, H.Y., 2015. Superhydrophobic and oleophobic surfaces obtained by graft copolymerization of perfluoroalkyl ethyl acrylate onto SBR rubber. Colloids Surf., A 481, 537–546.
Gao, Z.X., Zhai, X.L., Liu, F., et al, 2015. Fabrication of TiO_2/EP super-hydrophobic thin film on filter paper surface. Carbohydr. Polym. 128, 28–31.
Spathi, C., Young, N., Heng, J., et al, 2015. A simple method for preparing super-hydrophobic powder from paper sludge ash. Mater. Lett. 142, 80–83.
Zhang, Y.L., Hu, Z.M., Wang, Y., 2015. Super hydrophobic properties of papers prepared from multi-walled carbon nanotubes functionalized with polybenzimidazole and AgNPs. Mater. Sci. Forum 815, 629–633.
Navarro, F., Davalos, F., Dávalos, F., et al, 2003. Highly hydrophobic sisal chemithermomechanical pulp (CTMP) paper by fluorotrimethylsilane plasma treatment. Cellulose 10 (4), 411–424.
Song, Z., Xiao, H., Zhao, Y., 2014. Hydrophobic-modified nano-cellulose fiber/PLA biodegradable composites for lowering water vapor transmission rate (WVTR) of paper. Carbohydr. Polym. 111, 442–448.
Jonhed, A., Andersson, C., Jaernstroem, L., 2010. Effects of film forming and hydrophobic properties of starches on surface sized packaging paper. Packaging Technol. Sci. 21 (3), 123–135.
Cusola, O., Valls, C., Vidal, T., et al, 2013. Application of surface enzyme treatments using laccase and a hydrophobic compound to paper-based medi. Bioresour. Technol. 131, 521–526.
Cappelletto, E., Callone, E., Campostrini, R., et al, 2012. Hydrophobic siloxane paper coatings: The effect of increasing methyl substitution. J. Sol-Gel Sci. Technol. 62 (3), 441–452.
Jyoti, Y., Manali, D., Singh, G.V., 2014. Developing hydrophobic paper as a packaging material using epicuticular wax: A sustainable approach. Bioresources 9 (3), 5066–5072.
Iselau, F., Restorp, P., Andersson, M., et al, 2015. Role of the aggregation behavior of hydrophobic particles in paper surface hydrophobation. Colloids Surf., A 483, 264–270.
Oh, M.J., Lee, S.Y., Paik, K.H., 2011. Preparation of hydrophobic self-assembled monolayers on paper surface with silanes. J. Ind. Eng. Chem. 17 (1), 149–153.
Baidya, A., Ganayee, M.A., Swathy, J.R., et al, 2017. Organic solvent-free fabrication of durable and multifunctional superhydrophobic paper from waterborne fluorinated cellulose nanofiber building blocks. ACS Nano 11 (11), 11091–11099.
Liu, T.L., Chen, Z., Kim, C.J., 2015. A dynamic Cassie-Baxter model. Soft Matter 11 (8), 1589–1596.
Hisler, V., Vonna, L., Nardin, M., et al, 2014. Model experimental study of scale invariant wetting behaviors in Cassie-Baxter and Wenzel Regimes. Langmuir 30 (31), 9378–9383.
Erbil, H.Y., Cansoy, C.E., 2009. Range of applicability of the Wenzel and Cassie-Baxter equations for superhydrophobic surfaces. Langmuir 26 (24), 14135–14145.
Bhushan, B., Jung, Y.C., 2011. Natural and biomimetic artificial surfaces for superhydrophobicity, self-cleaning, low adhesion, and drag reduction. Prog. Mater Sci. 56, 1–108.
Sun, H., Liu, Y.J., Dan, L., et al, 2019. Hydrophobic SiO_2 nanoparticle-induced polyvinylidene fluoride crystal phase inversion to enhance permeability of thin film composite membrane. J. Appl. Polym. Sci. 136 (45), 48204.
Ye, H., Zhu, L.Q., Li, W.P., et al, 2016. Constructing fluorine-free and cost-effective superhydrophobic surface with normal-alcohol-modified hydrophobic SiO_2 nanoparticles. ACS Appl. Mater. Interfaces 9 (1), 1–26.
Mousavand, T., Ohara, S., Naka, T., et al, 2010. Organic-ligand-assisted hydrothermal synthesis of ultrafine and hydrophobic ZnO nanoparticles. J. Mater. Res. 25 (2), 219–223.
Ogihara, H., Jing, X., Okagaki, J., et al, 2012. Simple method for preparing superhydrophobic paper: spray-deposited hydrophobic silica nanoparticle coatings exhibit high water-Repellency and transparency. Langmuir 28 (10), 4605–4608.
Liang, Y.Y., Ju, J.G., Deng, N.P., et al, 2018. Super-hydrophobic self-cleaning bead-like SiO_2@PTFE nanofiber membranes for waterproof-breathable applications. Appl. Surf. Sci. 442, 54–64.
Xu, B., Cai, Z.S., Wang, W.M., et al, 2010. Preparation of superhydrophobic cotton fabrics based on SiO_2 nanoparticles and ZnO nanorod arrays with subsequent hydrophobic modification. Surf. Coat. Technol. 204 (9–10), 1556–1561.
Ranjbar, M., Taher, M.A., Sam, A., 2015. Facile single-step synthesis of SiO_2-coated ZnO nanorod as hydrophobic layer by hydrothermal method. J. Cluster Sci. 27 (1), 105–114.
Shirtcliffe, N.J., McHale, G., Atherton, S., et al, 2010. An introduction to superhydrophobicity. Adv. Colloid Interface Sci. 161, 124–138.
Erbil, H.Y., 2020. Practical applications of superhydrophobic materials and coatings: problems and perspectives. Langmuir 36, 2493–2509.
Khaghanpour, Z., Naghibi, S., 2017. Perforated ZnO nanoflakes as a new feature of ZnO achieved by the hydrothermal-assisted sol–gel technique. J. Nanostruct. Chem. 7, 55–59.